Environmental Technology & Innovation 9 (2018) 275–284

Contents lists available at ScienceDirect

Environmental Technology & Innovation

journal homepage: www.elsevier.com/locate/eti

Dynamics of mercury solid phase extraction using *Barbula lambarenensis*

Paul N. Diagboya *, Ezekiel D. Dikio

Department of Chemistry, Vaal University of Technology, Vanderbijlpark, South Africa

HIGHLIGHTS

- Low-cost (Barbula lambarenensis) adsorbent was utilized for water treatment.
- Aqueous Hg(II) ions were removed via biosorption studies.
- This biosorbent is better than most biosorbents in literature.
- Increase in aqueous temperature reduced Hg(II) adsorption: 303 $\geq$ 293 $>$ 313 K.

ARTICLE INFO

Article history:
Received 16 September 2017
Received in revised form 3 January 2018
Accepted 8 January 2018
Available online 16 January 2018

Keywords:
Mercury
Biosorption
Barbula lambarenensis
Kinetic
Isotherms

ABSTRACT

Water pollution and the attendant difficulty in developing viable local treatment techniques are major challenges in most countries. To address this, recent studies have focused on utilization of available low-cost adsorbents. However, a major limitation is their low adsorption capacities. Hence, we evaluated the effectiveness of naturally ubiquitous *Barbula lambarenensis* (RBL) for removal of aqueous Hg(II) ions via batch biosorption process. Biosorption was carried out at different temperatures (293–313 K), time (5–180 min), pH (3–7) and concentrations (20–60 mg/L), and data generated were explained using various kinetic and adsorption isotherm models. Results showed that equilibrium was attained in 120 min at 313 K and lower temperatures but faster at higher temperatures. However increase in temperature does not correspondingly lead to higher biosorption: 303 $\geq$ 293 $>$ 313 K. Optimum pH of adsorption was observed at 5.5. Modeling of the experimental data suggested that the biosorption process was majorly a monolayer surface phenomenon which occurred via sharing or exchange of valance electrons, and the RBL maximum adsorption capacity is 4.5 mg/g. The process was exothermic and spontaneous. Hydroxyl, carboxyl, thioesters and amide functional groups were implicated in the biosorption process. Overall, the study suggest that RBL may be useful for Hg(II) biosorption from aqueous solutions.

1. Introduction

In recent years, contamination of ground and surface waters has elicited a great deal of public health concern because of the importance of water in global development issues such as food security and global burden of disease (Okoli et al., 2014, 2016; Olu-Owolabi et al., 2017, 2014). Toxic metals such as Pb, Hg, Cr and Cd are of high priority because they are among the most ubiquitous environmental contaminants. These toxic metals are non-biodegradable, accumulate easily in biota, and

* Corresponding author.
E-mail address: pauld@vut.ac.za (P.N. Diagboya).

https://doi.org/10.1016/j.eti.2018.01.002
2352-1864/

cause myriads of health disorders in human (Daraei et al., 2014; Mohammad et al., 2010). For instance, the adverse impact of mercury (Hg) on biota is particularly intriguing because even at trace concentration, it could result in dysfunctional organs such as in the reproductive, cardiovascular and nervous systems (Diagboya et al., 2015). The occurrences of these metals in wastewaters from various anthropogenic activities have contributed to their ambient natural quantities in the environment. Since these metals ultimately find their way into water sources, there is need to cleanup wastewater so as to reduce the quantities of these metals that get into the environment.

At a minute concentration of approximately 6 ppb (0.006 mg/L), Hg is considered one of the most toxic metals (Diagboya et al., 2015). It occurs in the environment mainly as methyl mercury, a compound that is readily absorbed (>95%) by biota leading to its accumulation in the food chain (Hong et al. 2012; Shin and Han, 2012). Mercury or methyl mercury is not known to be useful to plants or animals (Hong et al., 2012). Adverse effects of Hg on biota are well documented; a well known case is the Hg poisoning in Minamata, Japan in 1956 (Diagboya et al., 2015; Hong et al., 2012; Shin and Han, 2012). Considering the recent reported increasing cases of Hg in the environment (Sunderland and Selin, 2013) and humans (Shin and Han, 2012) due to the recent industrial boom especially in the Asian subcontinent (Diagboya et al., 2015) and heavy mining areas of Africa, it is vital to reduce to the lowest possible concentration Hg in water.

Several techniques have been studied for the removal of contaminants from aqueous solutions, and these include physical, chemical, and combinations of both physical and chemical techniques. However, most of the techniques are plagued by techno-economic factors such as cost, inaccessibility and complex technologies (Olu-Owolabi et al., 2016a). The quest for new and locally available technologies has led to focus on biosorbents which are easy-to-handle, environmental-friendly and economically feasible (Okoli et al., 2015). Different kinds of plant biomasses have been investigated (Ibrahim et al., 2010; Kurniawan et al., 2006; Okoli et al., 2016; Olu-Owolabi et al., 2018; Pehlivan et al., 2009b; Saeed et al., 2009), but lower plants are ubiquitous and showing potential for removal of these toxic metals from water (Yang and Chen, 2008). *Barbula Lambarenensis* (RBL) is a common lower plant in sub-Saharan Africa, and it has been recognized, along with other lower plants, in the natural environment as bio-accumulators and bio-indicators of toxic metals pollution (Ogunfowokan et al., 2004). Despite this fact, RBL has been given little attention for water treatment purposes. Hence the objective of this study was to investigate the dynamics of solid phase extraction by using *Barbula lambarenensis* (RBL) for removal of Hg from aqueous solution.

2. Materials and methods

2.1. Biosorbent preparation and characterization

The sampled biomass of RBL was washed severally with deionized water to remove dirt. It was then air-dried followed by oven drying, pulverized using a steel blender, and sieved through a 230 mesh size sieve. The sieved particles were stored for this study. Physical and chemical characterizations were then carried out on the sieved samples. The surface area sample was determined using the method of Sears (1956), while the BET Specific Surface Area (SSA) (as well as Langmuir surface area (m^2/g), average pore size (nm), and Pore volume (cm^3/g)) was determined using Micromeritics ASAP 2020 M + C accelerated surface area and porosimetry analyzer (Micromeritics Instrument Corporation, USA). The bulk density and specific gravity were determined following the method described by Olu-Owolabi et al. (2012) and Okoli et al. (2016). The bulk density was obtained from the specific dry mass of the biomass to that of an equivalent volume of the same mass, while the specific gravity was obtained from the ratio of the same mass to an equivalent mass of water. The point of zero charge (pH_{PZC}) was determined using the solid addition method (Olu-Owolabi et al., 2018); by adding 0.1 g of the biomass into various 20 mL 0.01 M KNO_3 solutions with pH adjusted from 3 to 11, followed by 24 h equilibration. A graph of initial pH versus the difference between the initial and final pH (Δ pH) was plotted and the pHpzc was determined as intercept on the horizontal axis. The Fourier Transform Infrared (FTIR) spectra was obtained in KBr tablets on a Perkin Elmer Spectrum 1 FTIR spectrophotometer in the scanning frequency range of 4500–500 cm^{-1}. Scanning electron microscope (SEM) images were obtained using a Hitachi S-4800 microscope (Hitachi Ltd., Japan) equipped with a Horiba energy dispersive X-ray spectrometer.

2.2. Biosorption experiments

The batch equilibrium adsorption procedure (Diagboya et al., 2016; Okoli et al., 2016) was used to carry out the adsorption Hg(II) on RBL biomass. The experiment for effect of pH on Hg(II) adsorption was done from pH 3 to 7, while the effects of time (5–180 min and 50 mg/L Hg(II)) and concentration (20–60 mg/L Hg(II)) were carried out at three temperatures (293, 303 and 313 K) at solution pH of 5.5 ± 0.2 using 100 mg of RBL biomass in each 10 mL vials. Except where otherwise stated, equilibrium time of 120 min was used for the experiments. During the adsorption experiment, the RBL/Hg(II) mixtures were incubated by shaking in a temperature controlled shaker at either of the above stated temperatures. The vials were withdrawn from the shaker at the appropriate time interval, followed by separation of the adsorbents from solution by centrifugation at 4000 rpm for 20 min. All experiments were carried out in duplicate. Mercury concentrations of the solutions were determined using Varian 710-ES ICP optical emission spectrometer.

The quantity of Hg(II) adsorbed in each case was calculated using Eq. (1).

$$q_e = \frac{(C_o - C_e)v}{m} \tag{1}$$

where q_e, C_o, and C_e are the amount of Hg(II) adsorbed (mg/g), the initial and final Hg(II) concentrations in the solution (mg/L), respectively; and v (L) and m (g) are the volume of solution and mass of RBL biomass used for each experiment, respectively.

The experimental data were described using four kinetics models [Lagergren, 1898 Pseudo-First Order (PFO) (Eq. (2)) and Pseudo-Second Order (PSO) (Eq. (3)), the Elovich (Eq. (4)) and the Weber and Morris, 1963 Intra-Particle Diffusion (IPD) (Eq. (5)) kinetics models].

$$\log(q_e - q_t) = \log q_e - \frac{k_1}{2.303}t \tag{2}$$

$$\frac{t}{q_t} = \frac{1}{k_2 q_e^2} + \frac{t}{q_e} \tag{3}$$

$$q_t = \frac{1}{\beta}\ln(\alpha\beta) + \frac{1}{\beta}\ln(t) \tag{4}$$

$$q_t = k_i(t^{1/2}) + C \tag{5}$$

where q_e and q_t are Hg(II) adsorbed (mg/g) at equilibrium and at time t, respectively; and k_1 (/min) and k_2(g/mg/min) are the rate constants of the PFO and PSO, respectively. The q_e and rate constants were calculated from the slope and intercept of the plots of $\log(q_e - q_t)$ *vs.* t; and $\frac{t}{q_t}$ *vs.* t for PFO and PSO, respectively, α is the initial adsorption rate (mg/g/min) and β is the desorption constant (g mg^{-1}) during any one experiment, and C ($\mu g\ g^{-1}$) values indicate the thickness of the boundary layer of Hg(II) ion adsorbed, and k_i (mg/g/$min^{1/2}$) is intra-particle diffusion rate constant of the control stage.

The Langmuir (1916) (Eq. (6)) and Freundlich (1906) (Eq. (7)) adsorption isotherm models were employed in describing the adsorption process.

$$C_e/q_e = 1/(Q_o b) + C_e/Q_o \tag{6}$$

$$\log q_e = \log K_f + 1/(n)\log C_e \tag{7}$$

where Q_o (mg/g) is the maximum adsorption capacity per unit weight of adsorbent, b is a solute–surface interaction energy-related parameter, q_e and C_e are same as above, k_f and $1/n$ are the Freundlich model capacity factor and the isotherm linearity parameter, respectively.

The thermodynamic parameters; enthalpy (ΔH°), entropy (ΔS°), Gibbs free energy (ΔG°) and equilibrium constant (K_c), were determined using the equilibrium biosorption data at 293, 303, and 313 K. The values of the K_c were first determined using Eq. (8) for all data points.

$$K_c = \frac{q_e}{C_e}. \tag{8}$$

The K_c values of each point were plotted against q_e values to obtain the values of K_c for each temperature. The *Ln* K_c values were then plotted against the reciprocal of the temperatures to obtain the parameters in Eq. (8).

$$\ln K_c = -\Delta H^\circ/RT - \Delta S^\circ/R. \tag{9}$$

The ΔG° values were determined from Eq. (10).

$$\Delta G^\circ = -RT\ln K_c. \tag{10}$$

3. Results and discussion

3.1. Physical and chemical parameters

Biosorbent particle sizes are usually heterogeneous in nature, thus for an effective evaluation of the adsorption capacity of any biosorbent it is vital to determine important physical and chemical parameters. In this vein, the characterization results are as shown in Figs. 1(a) and 2, and Table 1. The specific surface area of RBL has been determined as 11.4 g/cm^3, while the bulk density and specific gravity for the biomass were 0.4 g/cm and 0.2, respectively (Okoli et al., 2016; Olu-Owolabi et al., 2012). The study shows that the pHpzc value which marks the pH where the surface functional groups do not contribute to the pH of the solution (Sposito, 1989) was relatively higher compared to those recorded in literature for most biosorbents (Igberase et al., 2017b; Leyva-Ramos et al., 2005; Meena et al., 2007); suggesting that surplus basic functional groups may be available on the surface of the RBL biomass. The values for bulk density, specific gravity, as well as the surface characteristics as revealed in Table 1, shows that the RBL biomass is of reasonable potential for water treatment.

Earlier studies (Okoli et al., 2016; Olu-Owolabi et al., 2012) showed that RBL may be used successfully for the removal of heavy metals from aqueous solution. Thus an effort was made to identify the possible functional groups of RBL responsible for the metal removal from aqueous solution using the FTIR spectra of the biomass (Fig. 1). Fig. 1 shows a number of absorption peaks of RBL. The broad band at 3404 cm^{-1} is indicative of a stretching vibration of free hydroxyl functional groups of different origins, and possibly N–H stretch of amides. The numerous free hydroxyl groups in the polysaccharide structure

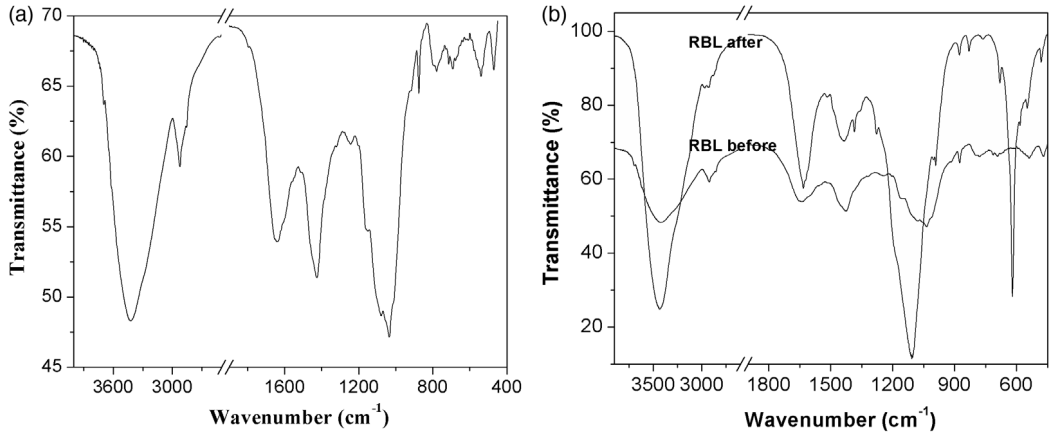

Fig. 1. (a) FTIR spectra of RBL (b) FTIR spectra of RBL before and after Hg^{2+} biosorption.

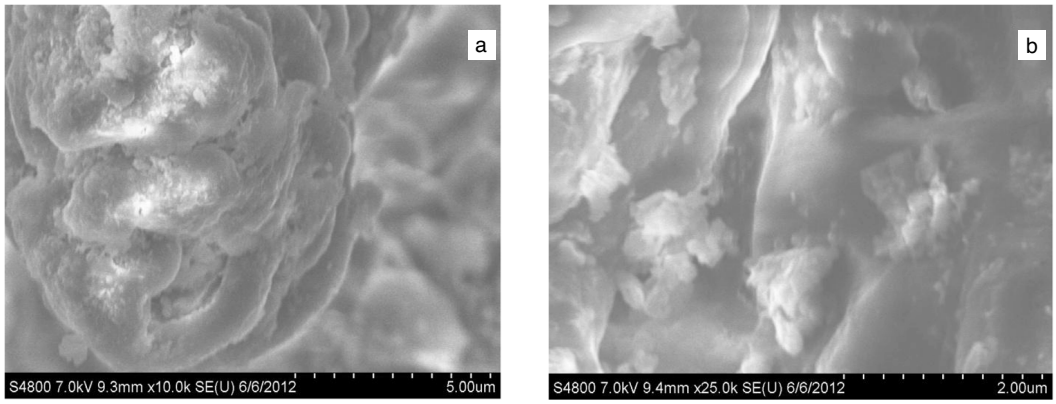

Fig. 2. RBL SEM surface morphology images [(a) 5.00 μm (b) 2.00 μm] before biosorption.

Table 1
Physico-chemical parameters of RBL.

Parameter	Value
BET Specific Surface Area (SSA) (m^2/g)	16.1
Surface area (g/cm^3)	11.4
Langmuir surface area (m^2/g)	48.5
Pore size (nm)	4.6
Pore volume (cm^3/g)	0.02
Bulk density (g/cm^3)	0.4
Specific gravity (m^2/g)	0.2
Point of zero charge (PZC)	7.0

of the RBL biomass cell wall may also explain the presence of this band. The absorption bands at 2919 and 2350 cm^{-1} are indicative of C–H in alkanes and the cumulative double bonds stretch of O=C=O, respectively. The band associated with free or esterified carboxyl groups (C=O stretch of carbonyl double bond) was observed at around 1700 cm^{-1}. Other peaks were observed at 1635 cm^{-1} (amide-I band of protein secondary structures) (Igberase et al., 2017a), 1425 cm^{-1} (aromatic methyl group/methyl ketone and carboxylate vibrations or likely C–H deformations of alkanes), 1041 cm^{-1} (C–OH bond and –C–C– stretchings of polysaccharides), below 1000 cm^{-1} (groups such as aromatic C–H bending vibrations, thioesters, and majorly plane deformations). Thus, the major functional groups implicated in RBL adsorption of metals are carboxylic acids, amides, thioesters and amide groups of protein. Similar observations have been reported by Chakravarty et al. (2010), Okoli et al. (2016), Yao et al. (2010), and Pehlivan et al. (2009a).

3.2. Comparison of adsorbent before and after biosorption studies

The infra-red spectra of the Hg(II)-loaded and unloaded RBL were compared (Fig. 1(b)). It was observed that the Hg(II)-loaded RBL spectra shows shifts as well as increase in intensity of spectra peaks (especially for OH^- and COO^- groups). It

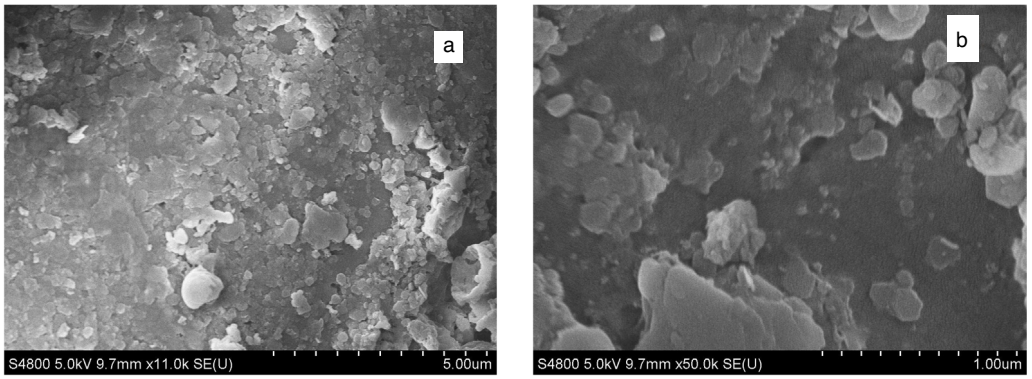

Fig. 3. RBL SEM surface morphology images [(a) 5.00 μm (b) 1.00 μm] after biosorption.

was observed that the amide-I band at 1635 cm^{-1} shifted to 1639 cm^{-1}, while the hydroxyl vibration at 1425 cm^{-1} shifted to 1436 cm^{-1}. The peaks at 3404, 1041 and 670 cm^{-1} shifted to 3448, 1111 and 621 cm^{-1}, respectively. These peaks were attributed to the biosorption of Hg(II) on the associated functional groups, and may be linked to the counter ions changes associated with these functional groups anions after the adsorption of Hg(II); and hence, indicate of the roles played by these RBL surface functional groups in the biosorption process. RBL SEM surface morphology images in Fig. 3 shows that the surfaces were covered with the adsorbed Hg(II) ions after biosorption as compared with Fig. 2 having rough surfaces which were involved in the biosorption process.

3.3. Mercury biosorption studies: effects of time and pH

In order to understand the efficiency of RBL for the adsorption of Hg(II) and the kinetics of the process under a set of prescribed conditions, the rate study is important. Hence, the batch equilibrium procedure was used to study the RBL Hg(II) adsorption rate and kinetics at pH 5.5 ± 0.2 and three temperatures – 293, 303, and 313 K – using Hg(II) concentration of 50 mg/L and RBL mass of 50 mg in the time range of 5–180 min. Fig. 4(a) shows trend curves of the effect of adsorption times on the biosorption of Hg(II) at all three temperatures. The steeper portions of the curve (circled) represents adsorption prior to equilibrium where the rate of adsorption is assumed to exceed desorption. At equilibrium (uncircled portion), the rates of adsorption and desorption are insignificantly different and the curve is virtually horizontal. The Figure shows that the Hg(II) adsorption rate within 30 min of the beginning of the adsorption experiment was relatively fast (compared to the remaining time) with over 75% of the adsorption occurring here. Hg(II) adsorption equilibrium was attained in 120 min at 293 and 303 K, while the equilibrium time decreased to 60 min at 313 K.

The pH of optimal Hg(II) biosorption is an another important parameter to be ascertained in order to determine the efficiency of RBL as an adsorbent for Hg(II). This is due to the fact that pH affects ionizable functional groups on a biosorbent surface and determines the charge on the aqueous pollutant (Okoli et al., 2016; Olu-Owolabi et al., 2016b). Thus the effect of pH on the biosorption of Hg(II) from solution has been carried out by equilibrating the RBL for 120 min in the solution pH range of 3–7. Result (Fig. 4(b)) showed that the biosorption process was pH dependent; amount of Hg(II) adsorbed increased with pH until optimum pH. This observation may be explained in the following manner. At the acidic pH region; less than 5, the amount of ionized functional groups on the surface of the RBL biomass was low, resulting in the reduced adsorption recorded. The reduced adsorption was due to effective competition between Hg(II) ions and protons in solution for the same negatively charged surface functional groups. Increase in the solution pH led to decrease of the protons in solution, and consequently less effective competition and higher number of negatively charged surface functional groups. This resulted in the higher biosorption observed. The increase in biosorption was observed until the pH 5.5 where no further increase in biosorption was observed. Subsequent experiments were carried out at pH 5.5.

It was observed from Fig. 4(a) that increase in Hg(II) solution temperature from 293 to 313 K did not lead to a corresponding increase in Hg(II) adsorption; in fact only a slight increase was noticed upon temperature increase from 293 to 303 K, however further increase reduced the Hg(II) biosorption by about 2%. The biosorption trend was 303 K $\geq$293 K $>$313 K. This trend shows that Hg(II) adsorption may be inversely proportional to the temperature. Diagboya et al. (2015), Olson et al. (2000) and Vidic and Siler (2001) have reported similar trend for Hg(II) adsorption. This trend may imply that the process of adsorption of Hg(II) on the RBL biomass material is exothermic and occurs by physisorption. The trend might be attributed to the fact that the metal, Hg, is liquid and volatile at room temperature, and increasing the ambient temperature increases the kinetic energy of the molecules in solution leading to the subsequent movement of the Hg(II) ions away from the adsorption surfaces, and hence the reduction in adsorption as temperature increased (Diagboya et al., 2015).

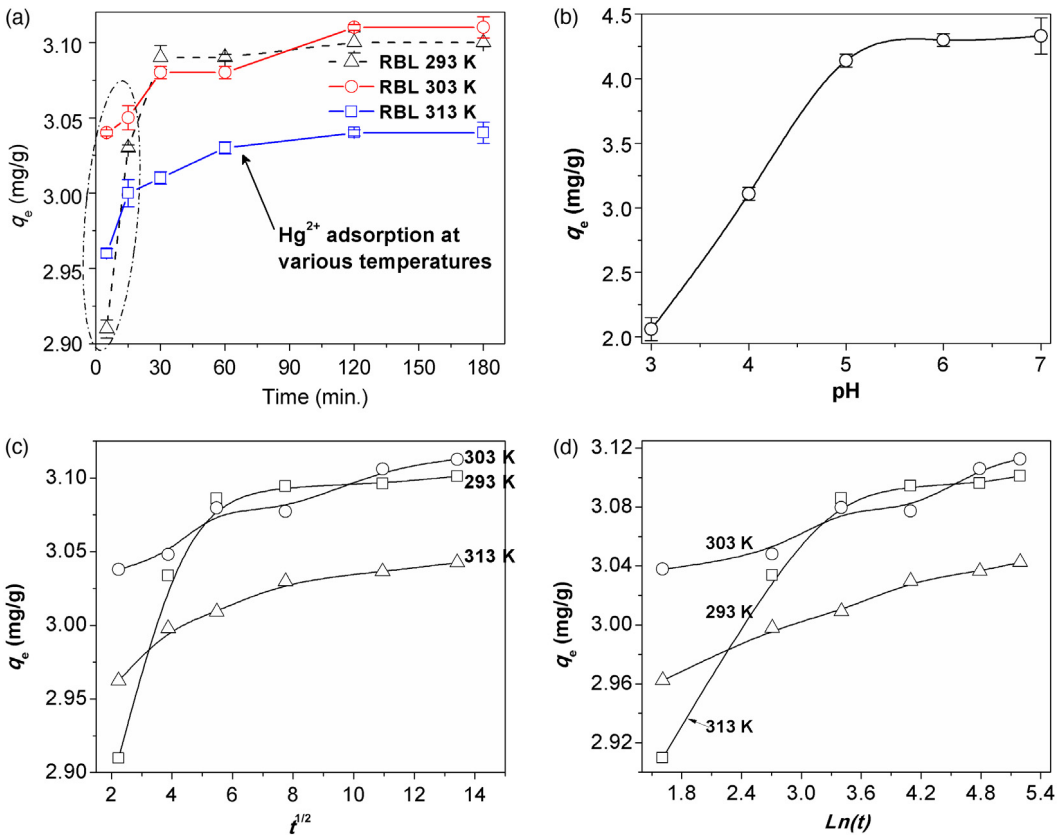

Fig. 4. (a) Effect of adsorption time on the biosorption of Hg(II) at all three temperatures; (b) effect of pH on Hg(II) biosorption; (c) intra-particle diffusion, and (d) Elovich kinetics model plots for Hg(II) biosorption at the three temperatures.

Table 2
Kinetics model parameters for Hg(II) biosorption on RBL.

	PFO			PSO			IPD			Elovich		Eq_e (mg/g)
	q_e (mg/g)	k_1 (/min)	r^2	q_e (mg/g)	k_2 (g/g/min)	r^2	k_t	C (mg/g)	r^2	β	r^2	
293 K	0.11	0.007	0.54	3.11	1.10	0.99	0.013	2.96	0.57	20.4	0.79	3.10
303 K	0.09	0.007	0.93	3.13	0.87	0.99	0.006	3.03	0.92	47.6	0.94	3.11
313 K	0.15	0.002	0.76	3.05	1.25	0.99	0.006	2.97	0.84	45.5	0.97	3.04

* Eq_e — Experimental q_e values.

3.4. Kinetics modeling studies

Adsorption data was described using the PFO and PSO kinetics models as well as the Elovich and IPD models. Calculated parameters for these models obtained by using the Hg(II) adsorption data at 293, 303, and 313 K are shown in Table 2, and these were used to predict the adsorption mechanism(s) involved in the RBL Hg(II) uptake. Comparison of the model RBL adsorption capacity (q_e) values (as well as the correlation coefficient $-r^2$ values) of the PFO and PSO models suggested that Hg(II) adsorption fit the PSO better (with r^2values closer to unity, $\geq$0.999) for all three temperatures; the experimental q_e values were also better correlated with the calculated model q_e values. This might be an indication that the adsorption of Hg(II) on the RBL adsorbent involved sharing or exchange of electrons between surface functional groups (such as hydroxyl, carboxyl, thioesters and amide groups) of the adsorbent and the cationic Hg(II) species in solution (Diagboya et al., 2014).

The IPD kinetics model parameters and plot are shown in Table 2 and Fig. 4(c), respectively. The plot of q_t versus $t^{1/2}$shows an initial linear but steep and rapid portion depicting over 85% of the curve, and a later horizontal portion for the remaining ($\leq$15%). The earlier portion suggests that intra-particle diffusion was the main adsorption mechanism in the first 100 min. The later portions of the plots suggested slow adsorption which was mainly controlled by equilibrium diffusion mechanism where the adsorption and desorption rates do not vary significantly. The C (mg/g) value of the IPD model suggests the thickness of the adsorbed Hg(II) at the surface of the RBL (Diagboya et al., 2014); and the values in Table 2 shows that over 95% of the adsorption occurred at the surface of the RBL. This conclusion may be drawn because C values significantly

Table 3
Comparison of Hg(II) adsorption on RBL with other adsorbents in literature.

Adsorbent	q_e (mg/g)	Reference
RBL	3.10	Present study
Allium sativum	0.65	Eom et al. (2011)
BPL-C[a]	0.37	Vidic and Siler (2001)
BPL-T[b]	1.25	Vidic and Siler (2001)
BPL-A[c]	0.30	Vidic and Siler (2001)
Graphene oxide	2.9	Diagboya et al. (2015)
Nauclea diderrichii	4.39	Omorogie et al. (2012)
Sago waste activated carbon	55.6	Kadirvelu et al. (2004)
GOMNP	16.6	Diagboya et al. (2015)
RGO–MnO_2	9.0	Sreeprasad et al. (2011)

[a] Commercially activated carbon impregnated with Cu—BPL-C.
[b] BPL-T—BPL impregnated with 2-aminoethanethiol.
[c] BPL-A—BPL impregnated with β-aminoanthraquinone.

Table 4
Hg(II) Adsorption isotherm models parameters.

Adsorption isotherm model	Parameter	293 K	303 K	313 K
Langmuir	Q_o (mg g^{-1})*	4.72	4.63	4.74
	β	1.01	3.38	0.70
	r^2	0.996	0.997	0.979
Freundlich	$1/n$	0.252	0.183	0.316
	k_f	2.74	3.18	2.10
	r^2	0.660	0.484	0.561

* Experimental *qe* value is 4.50 ± 0.10 mg/g.

correlated to the experimental q_e values. This implied that the Hg(II) removal process was mainly a surface phenomenon (adsorption). The *C* and high r^2 values of the IPD model also implied that the overall rate of the Hg(II) adsorption on RBL was dominated by surface intra-particle diffusion at the various temperatures.

The r^2 values of the Elovich kinetics model shows that the adsorption data may be explained by the model especially at higher temperatures (Table 2). This model which originated from chemical reaction kinetics suggested that there was some degree of boundary layer control between the Hg(II) ions and the RBL surface active adsorption sites since the curves (Fig. 4(d)) is not a straight line passing through the origin Tofighy and Mohammadi (2011). This control is assumed to be related to the rate determining mechanism and involved sharing of valence electron between the Hg(II) and RBL surface active adsorption sites.

In order to evaluate the effectiveness of the RBL adsorbent for aqueous Hg(II) removal, Hg(II) adsorption on the RBL was compared to some other adsorbents reported in literature at room temperature (Table 3). It was observed that though the pristine adsorbents may be sufficient to treat mercury pollution at the low concentration generally encountered in water, for higher concentration (as observed in some industries waste water), modification of the adsorbent may be more beneficial.

3.5. Equilibrium studies

Equilibrium biosorption studies for the process were carried out at three temperatures (293, 303, and 313 K) and results are represented in Fig. 5(a). Results showed that the biosorption of Hg(II) increased as concentration at all temperatures until all available biosorption sites were saturated and further biosorption was not permissible with increase in concentration. Similar to the results obtained for the effect of time, it was also observed that the biosorption increased as temperature was raised from 293 to 303 but further increase in temperature resulted in lower Hg(II) biosorption. The Hg(II) biosorption trend was 303 K $\geq$293 K >313 K. Similar trend has been reported by other workers (Diagboya et al., 2015; Olson et al., 2000; Vidic and Siler, 2001) for Hg(II) adsorption.

Equilibrium biosorption data have been fitted to the Langmuir and Freundlich adsorption isotherm models (Table 4; Fig. 5(c)–(d)). It was observed that the data fitted the Langmuir adsorption isotherm model better than the Freundlich. The Langmuir had correlation coefficient (r^2) values which were very close to unity as well as calculated maximum adsorption capacity (Q_o) values (≈4.6 mg/g) which were close to experimental q_e values (≈4.5 mg/g). The good fit of the data to the Langmuir adsorption isotherm model indicates that the biosorption process was on adsorption sites which possessed equal affinity for the Hg(II) ions, and formed only monolayer of the Hg(II) ions on the biosorbent surface at saturation. This was unlike the Freundlich isotherm model which assumes Hg(II) adsorption on heterogeneous surfaces with possible interactions between Hg(II) ions on the adsorption surfaces and those in solution.

The observed biosorption trend may imply that the Hg(II) biosorption process on the RBL biomass material was exothermic; hence, in order to understand the thermodynamics, the equilibrium data obtained at the different temperatures

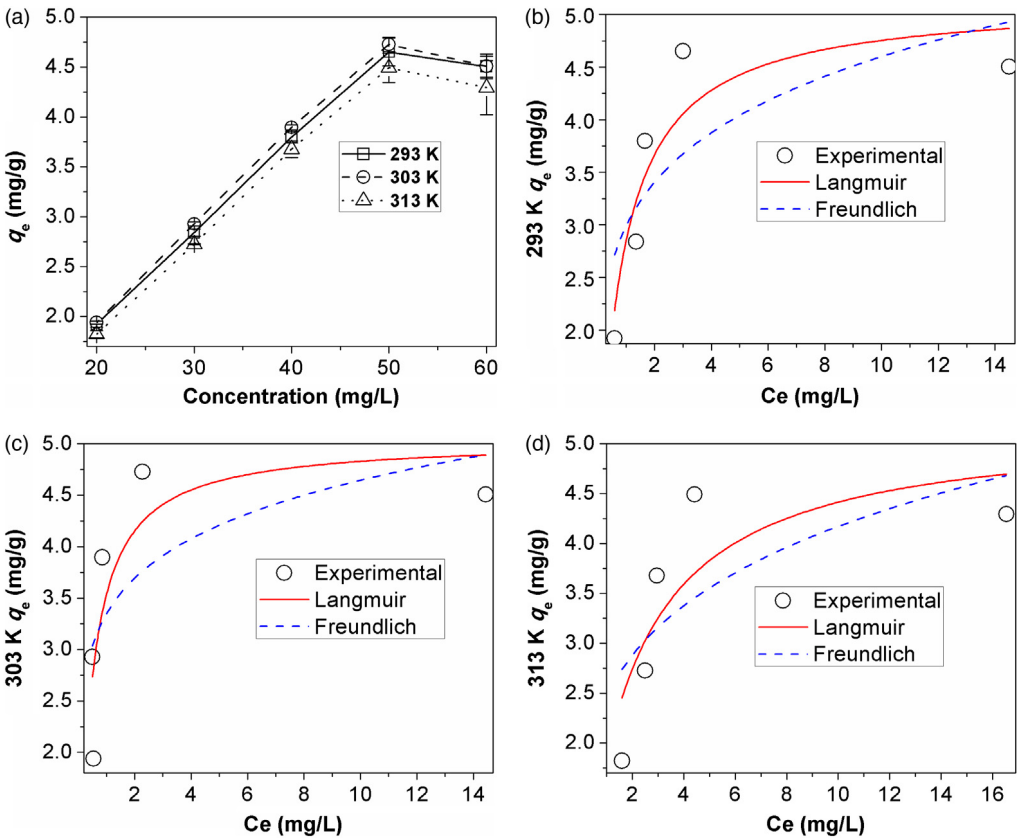

Fig. 5. Adsorption isotherm model plots for the adsorption of Hg(II) onto the RBL biomass.

Table 5
Thermodynamic parameters for Hg(II) biosorption.

	293 K	303 K	313 K
$\Delta G°$ (kJ/mol)	−3.78	−5.03	−1.11
$\Delta H°$ (kJ/mol)	−42.07	−42.07	−42.07
$\Delta S°$ (J/mol/K)	127.90	127.90	127.90

(293, 303, and 313 K) for the biosorption of Hg(II) have been used to generate the thermodynamic parameters ($\Delta G°$, $\Delta H°$, and $\Delta S°$) as shown in Table 5. Results indicated that the biosorption process was exothermic (negative $\Delta H°$), hence, increase in solution temperature resulted in reduced Hg(II) biosorption. However, the slight increase in Hg(II) biosorption observed as temperature increased from 293 to 303 K may be attributed to the energy needed to overcome the initial repulsive forces hindering Hg(II) biosorption. Further temperature increase to 313 K resulted in lowered biosorption, and this was attributed to increased kinetic energy of Hg(II) ions in solution as temperature increased. Hence, the observed trend for Hg(II) biosorption is 293 >303 >313 K. The magnitude of the $\Delta H°$ values suggested that the type of force involved in Hg(II) ions removal was weak van der Waal-like force, probably electrostatic in nature. The positive $\Delta S°$ value was indicative of increased randomness at the solid–liquid boundary as the processes drifted towards equilibrium, while the negative $\Delta G°$ values showed a spontaneous biosorption processes.

4. Conclusion

The study showed that the moss plant *Barbula lambarenensis*, an ubiquitous lower plant in sub-Saharan Africa, can be used for Hg(II) removal from aqueous solution. RBL has Hg(II) adsorption capacity of 4.50 mg/g, while optimum adsorption was achieved after 120 min and pH 5.5. Higher temperatures reduced Hg(II) adsorption by RBL: 303 ≥293 >313 K. The kinetics models showed that Hg(II) adsorption was mainly a surface phenomenon and involved sharing or exchange of electrons between surface functional groups of RBL and the cationic Hg(II) species in solution. The Langmuir adsorption isotherm model suggested a surface monolayer Hg(II) biosorption. Thermodynamically, the biosorption process was exothermic and spontaneous. Hence, RBL may be useful for the removal of Hg(II) from aqueous solutions.

Acknowledgments

We acknowledge the supports of the Department of Chemistry and Research Directorate, Vaal University of Technology, Vanderbiljpark, South Africa, as well as the supports of the World Academy of Sciences (TWAS) and the Chinese Academy of Sciences (CAS) for the awards of CAS–TWAS postgraduate fellowship to P.N. Diagboya (FR no.: 3240255024).

References

Chakravarty, S., Mohanty, A., Sudha, T.N., Upadhyay, A.K., Konar, J., Sircar, J.K., Madhukar, A., Gupta, K.K., 2010. Removal of Pb(II) ions from aqueous solution by adsorption using bael leaves (Aegle marmelos). J. Hazard. Mater. 173 (1–3), 502–509.

Daraei, H., Mittal, A., Mittal, J., Kamali, H., 2014. Optimization of Cr(VI) removal onto biosorbent eggshell membrane: experimental and theoretical approaches. Desalin. Water Treat. 52, 1307–1315.

Diagboya, P.N., Olu-Owolabi, B.I., Adebowale, K.O., 2014. Microscale scavenging of pentachlorophenol in water using amine and tripolyphosphate-grafted SBA-15 silica: Batch and modeling studies. J. Environ. Manage. 146, 42–49.

Diagboya, P.N., Olu-Owolabi, B.I., Adebowale, K.O., 2015. Synthesis of covalently bonded graphene oxide–iron magnetic nanoparticles and its kinetics of mercury removal. RSC Adv. 5, 2536–2542.

Diagboya, P.N., Olu-Owolabi, B.I., Adebowale, K.O., 2016. Distribution and interactions of pentachlorophenol in soils: The roles of soil iron oxides and organic matter. J. Contam. Hydrol. 191, 99–106.

Eom, Y., Won, J.H., Ryu, J.-Y., Lee, T.G., 2011. Biosorption of mercury(II) ions from aqueous solution by garlic (Allium sativum L.) powder. Korean J. Chem. Eng. 28 (6), 1439–1443.

Freundlich, H.M.F., 1906. Über die adsorption in lösungen. Z. Phys. Chem. 57A, 385–470.

Hong, Y.-S., Kim, Y.-M., Lee, K.-E., 2012. Methylmercury exposure and health effects. J. Prev. Med. Public Health 45 (6), 353–363.

Ibrahim, M.N.M., Ngah, W.S.W., Norliyana, M.S., Daud, W.R.W., Rafatullah, M., Sulaiman, O., Hashim, R., 2010. A novel agricultural waste adsorbent for the removal of lead (II) ions from aqueous solutions. J. Hazard. Mater. 182 (1–3), 377–385.

Igberase, E., Osifo, P., Ofomaja, A., 2017a. Mathematical modelling of Pb2+, Cu2+, Ni2+, Zn2+, Cr6+ and Cd2+ ions adsorption from a synthetic acid mine drainage onto chitosan derivative in a packed bed column. Environ. Technol. 1–18.

Igberase, E., Osifo, P., Ofomaja, A., 2017b. Adsorption of metal ions by microwave assisted grafting of cross-linked chitosan beads. Equilibrium, isotherm, thermodynamic and desorption studies. Appl. Organometal. Chem. http://dx.doi.org/10.1002/aoc.4131.

Kadirvelu, K., Kavipriya, M., Karthika, C., Vennilamani, N., Pattabhi, S., 2004. Mercury (II) adsorption by activated carbon made from sago waste. Carbon 42, 745–752.

Kurniawan, T.A., Chan, G.Y.S., Lo, W., Babel, S., 2006. Comparisons of low-cost adsorbents for treating wastewaters laden with heavy metals. Sci. Total Environ. 366, 409–426.

Lagergren, S., 1898. Zur theorie der sogenannten adsorption gelöster stoffe. Kungl. Svenska Vetenskapsakademiens. Handlingar 24, 1–39.

Langmuir, I., 1916. The constitution and fundamental properties of solids and liquids. J. Amer. Chem. Soc. 38, 2221–2295.

Leyva-Ramos, R., Bernal-Jacome, L.A., Acosta-Rodriguez, I., 2005. Adsorption of Cd(II) from aqueous solution on natural and oxidized corncob. Sep. Purif. Technol. 45, 41–49.

Meena, A.K., Kadirvelu, K., Mishra, G.K., Rajagopal, C., Nagar, P.N., 2007. Adsorption of Pb(II) and Cd(II) metal ions from aqueous solutions by mustard husk. J. Hazard. Mater. 150, 619–625.

Mohammad, M., Maitra, S., Ahmad, N., Bustam, A., Sen, T.K., Dutta, B.K., 2010. Metal ion removal from aqueous solution using physic seed hull. J. Hazard. Mater. 179 (1–3), 363–372.

Ogunfowokan, A.O., Asubiojo, O.I., Adeniyi, A.A., Oluyemi, E.A., 2004. Trace Pb, Zn, and Cu in Barbula Lambarenensis as a monitor of local atmospheric pollution in Ile-Ife, Nigeria. J. Appl. Sci. 4, 380–383.

Okoli, C.P., Adewuyi, G.O., Zhang, Q., Diagboya, P.N., Guo, Q., 2014. Mechanism of dialkyl phthalates removal from aqueous solution using γ-cyclodextrin and starch based polyurethane polymer adsorbents. Carbohydr. Polym. 114, 440–449.

Okoli, C.P., Adewuyi, G.O., Zhang, Q., Zhu, G., Wang, C., Guo, Q., 2015. Aqueous scavenging of polycyclic aromatic hydrocarbons using epichlorohydrin, 1,6-hexamethylene diisocyanate and 4,4-methylene diphenyl diisocyanate modified starch: Pollution remediation approach. Arab. J. Chem. http://dx.doi.org/10.1016/j.arabjc.2015.06.004.

Okoli, C.P., Diagboya, P.N., Anigbogu, I.O., Olu-Owolabi, B.I., Adebowale, K.O., 2016. Competitive biosorption of Pb(II) and Cd(II) ions from aqueous solutions using chemically modified moss biomass (Barbula lambarenensis). Environ. Earth Sci. 76 (1).

Olson, E.S., Miller, S.J., Sharma, R.K., Dunham, G.E., Benson, S.A., 2000. Catalytic effects of carbon sorbents for mercury capture. J. Hazard. Mater. 74, 61–79.

Olu-Owolabi, B.I., Alabi, A.H., Diagboya, P.N., Unuabonah, E.I., Düring, R.-A., 2017. Adsorptive removal of 2,4,6-trichlorophenol in aqueous solution using calcined kaolinite-biomass composites. J. Environ. Manage. 192, 94–99.

Olu-Owolabi, B.I., Alabi, A.H., Unuabonah, E.I., Diagboya, P.N., Böhm, L., Düring, R.-A., 2016a. Calcined biomass-modified bentonite clay for removal of aqueous metal ions. J. Environ. Chem. Eng. 4 (1), 1376–1382.

Olu-Owolabi, B.I., Diagboya, P.N., Adebowale, K.O., 2014. Evaluation of pyrene sorption–desorption on tropical soils. J. Environ. Manage. 137, 1–9.

Olu-Owolabi, B.I., Diagboya, P.N., Ebaddan, W.C., 2012. Mechanism of Pb2+ removal from aqueous solution using a nonliving moss biomass. Chem. Eng. J. 195–196, 270–275.

Olu-Owolabi, B.I., Diagboya, P.N., Okoli, C.P., Adebowale, K.O., 2016b. Sorption behaviour of pentachlorophenol in sub-Saharan tropical soils: soil types sorption dynamics. Environ. Earth Sci. 75 (24).

Olu-Owolabi, B.I., Diagboya, P.N., Unuabonah, E.I., Alabi, A.H., Düring, R.-A., Adebowale, K.O., 2018. Fractal-like concepts for evaluation of toxic metals adsorption efficiency of feldspar-biomass composites. J. Clean. Prod. 171C, 884–891.

Omorogie, M.O., Babalola, J.O., Unuabonah, E.I., Gong, J.R., 2012. Kinetics and thermodynamics of heavy metal ions sequestration onto novel Nauclea diderrichii seed biomass. Bioresour. Technol. 118, 576–579.

Pehlivan, E., Altun, T., Cetin, S., Iqbal Bhanger, M., 2009a. Lead sorption by waste biomass of hazelnut and almond shell. J. Hazard. Mater. 167 (1–3), 1203–1208.

Pehlivan, E.,Özkan, A.M., Dinç, S., Parlayici, Ş., 2009b. Adsorption of Cu2+ and Pb2+ ion on dolomite powder. J. Hazard. Mater. 167 (1–3), 1044–1049.

Saeed, A., Iqbal, M., Höll, W.H., 2009. Kinetics, equilibrium and mechanism of Cd2+ removal from aqueous solution by mungbean husk. J. Hazard. Mater. 168 (2–3), 1467–1475.

Sears, G.W., 1956. Determination of specific surface area of colloidal silica by titration with sodium hydroxide. Anal. Chem. 28, 1981–1983.

Shin, S.-R., Han, A.L., 2012. Improved chronic fatigue symptoms after removal of mercury in patient with increased mercury concentration in hair toxic mineral assay: A case. Korean J. Fam. Med. 33 (5), 320.

Sposito, G., 1989. The Chemistry of Soils. Oxford University Press, New York, NY.

Sreeprasad, T.S., Maliyekkal, S.M., Lisha, K.P., Pradeep, T., 2011. Reduced graphene oxide–metal/metal oxide composites: Facile synthesis and application in water purification. J. Hazard. Mater. 186 (1), 921–931.
Sunderland, E.M., Selin, N.E., 2013. Future trends in environmental mercury concentrations: Implications for prevention strategies. Environ. Health. 12, 2.
Tofighy, M.A., Mohammadi, T., 2011. Adsorption of divalent heavy metal ions from water using carbon nanotube sheets. J. Hazard. Mater. 185 (1), 140–147.
Vidic, R.D., Siler, D.P., 2001. Vapor-phase elemental mercury adsorption by activated carbon impregnated with chloride and chelating agents. Carbon 39, 3–14.
Weber, W.J., Morris, J.C., 1963. Kinetics of adsorption on carbon from solutions. J. Sanit. Eng. Div., Am. Soc. Civil Eng. 89, 31–60.
Yang, L., Chen, P., 2008. Biosorption of hexavalent chromium onto intact and chemically modified Sargassum sp. Bioresour. Technol. 99, 297–307.
Yao, Z.Y., Qi, J.H., Wang, L.H., 2010. Equilibrium, kinetic and thermodynamic studies on the biosorption of Cu(II) onto chestnut shell. J. Hazard. Mater. 174 (1–3), 137–143.